Gate control of a quantum dot single-electron spin in realistic confining potentials: Anisotropy effects

Sanjay Prabhakar and James E. Raynolds
College of Nanoscale Science and Engineering, University at Albany, State University of New York, Albany, New York 12203, USA
(Received 26 November 2008; revised manuscript received 25 March 2009; published 5 May 2009)

Among recent proposals for next-generation non-charge-based logic is the notion that a single electron can be trapped and its spin can be manipulated through the application of gate potentials. In this paper, we present numerical simulations of such spins in single-electron devices for realistic (asymmetric) confining potentials in two-dimensional electrostatically confined quantum dots. Using analytical and numerical techniques we show that breaking the in-plane rotational symmetry of the confining potential leads to a significant effect on the tunability of the *g* factor with applied gate potentials. In particular, anisotropy extends the range of tunability to larger quantum dots.

DOI: 10.1103/PhysRevB.79.195307 PACS number(s): 73.21.La, 72.25.Hg, 73.63.Kv

I. INTRODUCTION

The notion of using single-electron spins for quantum computing and next-generation logic is an attractive idea that has received considerable attention in recent years.[1–13] In order to integrate new concepts with existing semiconductor technology, a number of researchers have recently explored the possibility of using *electric fields* generated by imposed gate potentials to manipulate single-electron spins in quantum dot devices.[14–34]

The goal of the present work is to utilize state-of-the-art numerical techniques to explore the fundamental physics of single-electron spin devices and to provide realistic information for the practical design of such systems. We utilize a finite-element based numerical technique to study electrostatically defined quantum dots that is similar to other recently published work.[35]

A key result of the present work is the discovery that spatial symmetry breaking[36–38] resulting from the anisotropy of realistic confining potentials results in an enhancement of the electric-field tunability of the electron *g* factor over that found for symmetric potentials for dots larger than roughly 65 nm.

Indeed, symmetry plays a key role in spin-orbit interactions in systems such as the one considered in this work. The Dresselhaus[39] and Bychkov and Rashba[40] coupling terms (discussed in detail below) are manifestations of the spin-orbit interaction arising due to bulk inversion asymmetry and the quantum well confining potential asymmetry, respectively. The forms of these interactions, given in Eqs. (18)–(20), are well established and have been used in many studies.[14–37]

It is also generally understood that the Zeeman splitting depends on the direction of an applied field and is thus described by a *g*-factor *tensor*.[19,38,41–43] Some authors have also explored the effects of asymmetry of the quantum dot confining potential in coupled quantum dot systems.[36,44–46] A subject that seems to have received little attention is the question of anisotropy effects in a single dot and is the subject of the present investigation.

Our approach is most closely related to that of Ref. 14 but differs in that we take a numerical approach based on the finite element method[47] whereas the authors of Ref. 14 use perturbation-theory and direct diagonalization techniques and did not consider anisotropy effects. Another recent work, similar to ours, employing real-space numerical (finite-difference) methods has also appeared.[35] This work was concerned with the determination of realistic self-consistent potentials, electron-electron interaction effects, and interaction with quantum point contacts. We now turn to a discussion of our computation method.

II. COMPUTATIONAL METHOD

We utilize a multiscale multiphysics simulation strategy based on the finite element method[47] to provide a realistic description of the physics of single-spin devices in three-dimensional geometries. The ideal is to solve self-consistently the Maxwell equations of electrostatics with the Schrödinger equation in three-dimensional geometry. Unfortunately such a solution is not feasible given currently available techniques due to the disparity of length scales in the problem. We thus seek an approximate solution that is built up in stages.

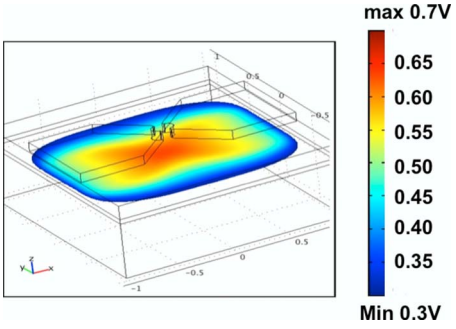

FIG. 1. (Color online) Electrostatic potential for a prototype single-electron device plotted in the 2DEG layer. This figure illustrates a single-spin device consisting of two triangular gates above a 2DEG. The gates were held at 1*V* and the 2DEG was held at 0*V*. For simplicity of the electrostatic calculation, the 2DEG was treated as a classical perfect conductor. The dimensions of the device in the *x* and *y* directions are 2.8 and 1.8 μm, respectively, and the thickness is 1 μm.

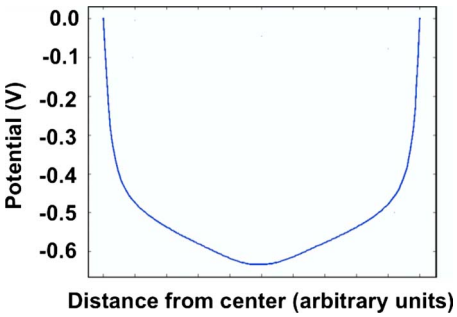

FIG. 2. (Color online) Electrostatic confining potential in the 2DEG along the symmetry axis of a prototype single-electron device. This figure was made by plotting the potential of Fig. 1 along a line in the 2DEG through the symmetry axis of the device (the x axis of Fig. 1, i.e., a line running from one gate to the other) intersecting with the central region.

In the first step of our approach, we construct a three-dimensional model of the device and calculate the gate-induced electrostatic potentials that cause the formation of a quantum dot in the two-dimensional electron gas (2DEG) at a AlGaAs/GaAs heterojunction as illustrated in Figs. 1–3. This geometry corresponds to prototype devices that are under consideration by experimentalists at the University at Albany, State University of New York.

In order to obtain the electrostatic solution for the confining potential, we approximate the 2DEG as a classical perfect conductor and give it a finite width. The width ($\approx$0.05 μm) is unrealistically large from a quantum perspective but is assumed to give a reasonable description of the spatial variation of the potential in the layer of the 2DEG. In a subsequent step we treat the 2DEG from a realistic quantum-mechanical perspective.[48]

Figures 2 and 3 are one-dimensional plots obtained from Fig. 1 by plotting the potential along a line in the 2DEG along high-symmetry directions. These one-dimensional potentials are then fit to polynomial forms $P_x(x)$ and $P_y(y)$. These are then used as a potential of the form

$$V_{\text{real}}(x,y) \approx P_x(x) + P_y(y) \tag{1}$$

to approximate the confining potential of the electron in the Schrödinger equation. Before considering electron motion in the above potential, V_{real}, we consider the simpler quadratic potential

$$V_{\text{quad}} \equiv \frac{1}{2} m\omega_o^2(\alpha x^2 + \beta y^2) \tag{2}$$

that allows for systematic studies. For convenience we have written the strength of the potential in harmonic-oscillator form by defining the prefactor $\frac{1}{2}m\omega_o^2$. The potential of Eq. (2) is a paraboloid of revolution and is commonly employed in model studies of two-dimensional (2D) quantum dots.[49] The separable form given in Eq. (1) is a generalization of Eq. (2) from quadratic to polynomial form and is an ansatz. It is assumed to give a good description of the system and the results of Figs. 6 and 11 support this hypothesis.

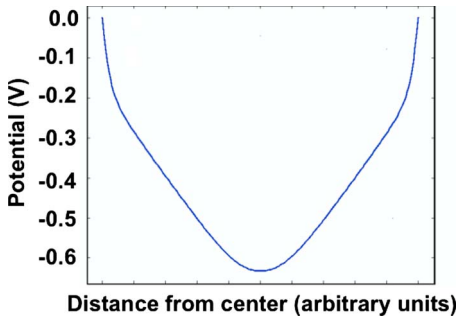

FIG. 3. (Color online) Electrostatic confining potential in the 2DEG normal to the symmetry axis of a prototype single-electron device. This figure was made by plotting the potential of Fig. 1 along a line in the 2DEG normal to the symmetry axis of the device (the y axis of Fig. 1) and intersecting the central region.

In the second step we calculate the wave functions and self-consistent potential at the heterojunction between AlGaAs and GaAs that describes the formation of the two-dimensional electron gas as illustrated in Fig. 4. We do this calculation primarily to benchmark our numerical method by making contact with a well-known result from the literature.[48]

The results of Fig. 4 are obtained by solving the following coupled equations that constitute the self-consistent Schrödinger-Poisson equations including exchange-correlation effects [see Eq. (5), and references that follow it]:

$$\frac{-\hbar^2}{2}\frac{d}{dz}\left(\frac{1}{m(z)}\frac{d\psi_i(z)}{dz}\right) + V(z)\psi_i(z) = E_i\psi_i(z), \tag{3}$$

$$\frac{d}{dz}\left(\epsilon_o\kappa(z)\frac{d\phi(z)}{dz}\right) = e\sum_i n_i|\psi_i(z)|^2 - \rho(z), \tag{4}$$

where $\kappa(z)$ and $\rho(z)$ are the fixed spatially dependent dielectric function and background charge density of the interface

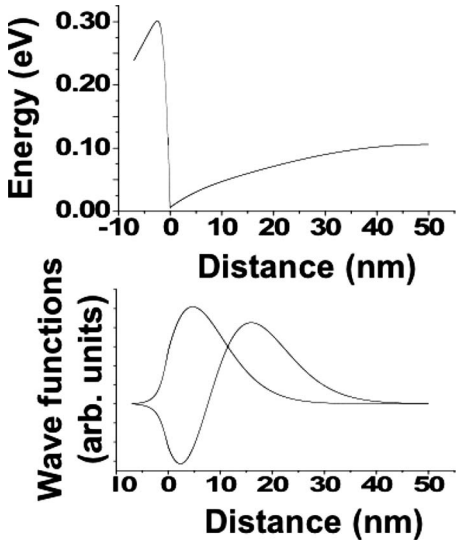

FIG. 4. Heterojunction self-consistent potential (upper panel) and lowest two wave functions (lower panel) of the 2DEG. These results demonstrate consistency of our results with other published work (Ref. 48).

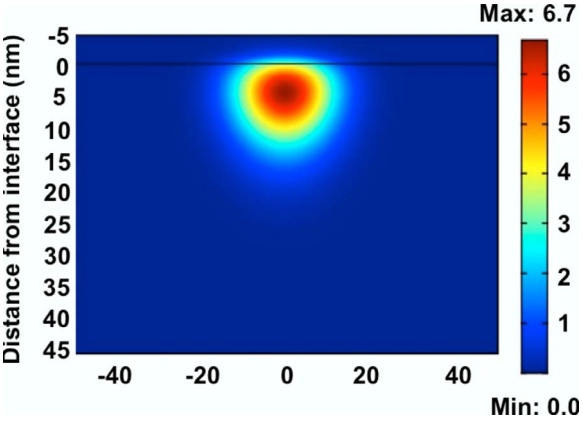

FIG. 5. (Color online) Quantum dot wave function plotted in the x-z plane formed by applying a quadratic confining potential in the plane (i.e., along the x axis). This potential is characterized by the parameter ℓ_o=20 nm [quantum dot radius, see Eq. (7)].

as described in Ref. 48. The potential energy of the 2DEG is given by

$$V(z) = -e\phi(z) + V_{\mathrm{xc}}(z), \tag{5}$$

where $\phi(z)$ is the self-consistent potential and $V_{\mathrm{xc}}(z)$ is the well-known Hedin and Lundqvist parametrization of the exchange-correlation potential given in Ref. 50 and reproduced as Eqs. (8)–(10) of Ref. 48. In the above equations, the coordinate z is measured relative to the interface between AlGaAs and GaAs. The results of Fig. 4 are in excellent agreement with previous results[48] confirming the soundness of our approach.

We next consider the formation of an electrostatically defined quantum dot by applying a symmetric, confining potential in the plane of the 2DEG as illustrated in Fig. 5. In other words, we add a potential of the form

$$V_x(x) = \frac{1}{2}m\omega_o^2 x^2 \tag{6}$$

to Eq. (5) and solve the system of Eqs. (3)–(5) self-consistently in the two-dimensional x-z domain. Figure 5 clearly illustrates the formation of a quantum dot in the potential well of the 2DEG as expected.

In the remainder of this paper we focus our attention on motion in the plane of the 2DEG and contrast effects associated with quantum dots in symmetric and asymmetric confining potentials as illustrated in Figs. 6(a) and 6(b), respectively. These figures were obtained using the quadratic model potential of Eq. (2) with $\alpha=\beta=1$ for the symmetric case [Fig. 6(a)] and $\alpha=1$ and $\beta=2.8$ for the asymmetric case [Fig. 6(b)], in the Hamiltonian, H_{xy}, describing motion in the two-dimensional plane of the 2DEG (i.e., x-y plane), to be discussed in the following. The quantum dot radius defined by

$$\ell_o \equiv \sqrt{\frac{\hbar}{m\omega_o}} \tag{7}$$

was chosen to have the value ℓ_o=30 nm.

The parameters of the asymmetric potential were chosen so as to mimic the realistic potential of Figs. 2 and 3. In other words, we obtain x_o and y_o as the solutions to the following equations:

$$\epsilon_o = P_x(x_o) \tag{8}$$

and

$$\epsilon_o = P_y(y_o), \tag{9}$$

where ϵ_o is the ground-state eigenvalue in the realistic potential of Eq. (1). We then fix the three parameters α, β, and ω_o as follows. As there are three parameters and two equations, we can choose one at will. We therefore take $\alpha=1$ throughout the rest of this paper. The ratio of α to β is then determined by taking the ratio of the following equations:

$$\epsilon_o = \frac{1}{2}m\omega_o^2 \alpha x_o^2 \tag{10}$$

and

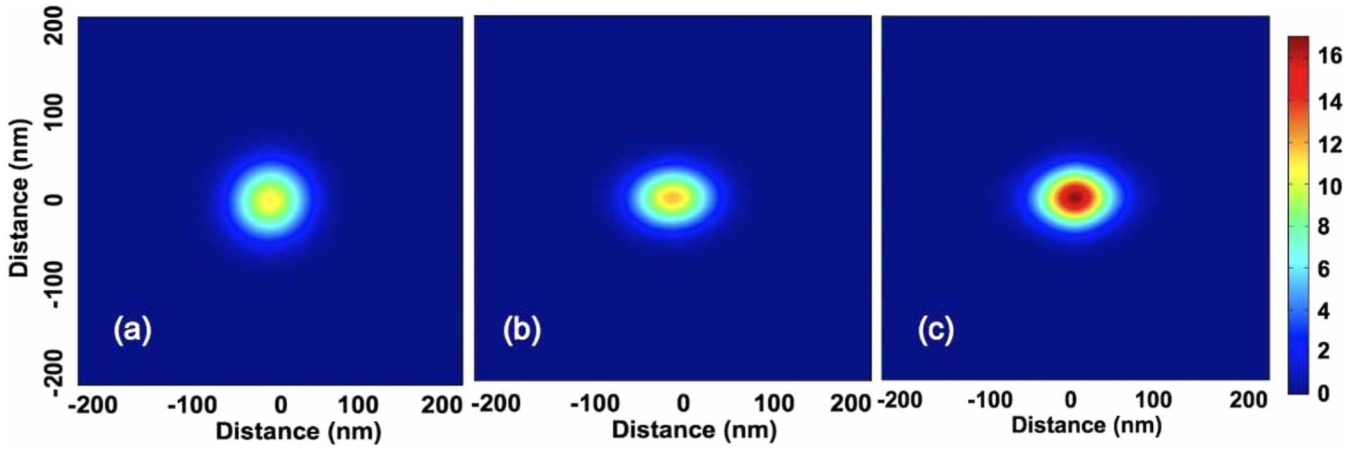

FIG. 6. (Color online) In-plane wave function for quantum dots formed by three potentials: (a) the symmetric quadratic model of Eq. (2) with $\alpha=\beta=1$ and ℓ_o=30 nm [see Eq. (7)]; (b) the asymmetric quadratic model of Eq. (2) with $\alpha=1$, $\beta=2.8$, and ℓ_o=30 nm; and (c) the realistic potential of Eq. (1) and Figs. 2 and 3.

$$\epsilon_o = \frac{1}{2} m \omega_o^2 \beta y_o^2, \tag{11}$$

to give $\beta = x_o^2 / y_o^2$. Lastly we choose ω_o as determined by the coefficient of the quadratic term in $P_y(y)$ (plotted in Fig. 3) [the polynomial $P_x(x)$ has no quadratic term]. The resulting values are $\beta = 2.8$ and the value of ω_o is most conveniently expressed equivalently by $\ell_o \approx 30$ nm. The wave function in the asymmetric model potential of Fig. 6(b) should be contrasted with the wave function in the realistic potential [i.e., using the form of Eq. (1)] as shown in Fig. 6(c) as will be discussed further in the remainder of this paper.

We consider the motion of the electron in the x-y plane of the quantum dot in the presence of a magnetic field oriented perpendicular to the plane of the 2DEG. Our approach closely follows that of Ref. 14. Thus the total Hamiltonian can be written as

$$H = H_{xy} + H_z + H_{\mathrm{so}}, \tag{12}$$

where H_z corresponds to motion normal to the interface [as discussed in the context of Eqs. (3)–(5)], H_{so} is the spin-orbit interaction to be discussed shortly, and the remaining term is given by

$$H_{xy} = \frac{\vec{P}^2}{2m} + \frac{1}{2} m \omega_o^2 (\alpha x^2 + \beta y^2) + \frac{1}{2} g_o \mu_B \sigma_z B, \tag{13}$$

where the kinetic momentum operator

$$\vec{P} \equiv \vec{p} + \frac{e}{c} \vec{A} \tag{14}$$

is the sum of the canonical momentum

$$\vec{p} \equiv -i\hbar(\partial_x, \partial_y, 0) \tag{15}$$

and the vector potential (in the symmetric gauge)

$$\vec{A} \equiv \frac{B}{2}(-y, x, 0). \tag{16}$$

The eigenstates of H_{xy} [Eq. (13)] with $\alpha = \beta$ are the well-known Fock-Darwin states.[51,52] The situation with $\alpha \neq \beta$ also has an analytic solution.[49] We have verified that our numerical solution of $H_{xy}|\psi\rangle = \epsilon|\psi\rangle$ is consistent with these analytical results.

Lastly we consider the spin-orbit interaction as embodied in the Hamiltonian H_{so} which is the essential ingredient in the phenomena of electric-field-induced spin switching.[6,14] We write

$$H_{\mathrm{so}} = H_R + H_{D1} + H_{D2}, \tag{17}$$

where the *Rashba* interaction[40,53] is given by

$$H_R = \frac{\alpha_R e E}{\hbar}(\sigma_x P_y - \sigma_y P_x) \tag{18}$$

and the linear and cubic *Dresselhaus* interactions[39,54] are written as

$$H_{D1} = \frac{0.7794 \gamma_c k^2}{\hbar}(-\sigma_x P_x + \sigma_y P_y), \tag{19}$$

which is linear in components of the momentum operator $\vec{P}$ and

$$H_{D2} = \frac{\gamma_c}{\hbar^3}(-\sigma_x P_x P_y^2 - \sigma_y P_y P_x^2) + \mathrm{H.c.}, \tag{20}$$

which is cubic in components of the momentum operator (H.c. denotes the Hermitian conjugate).[14] Note that the electric-field strength E that enters Eq. (18) is that associated with the heterojunction $|E| = \partial V(z)/\partial z$ and is treated as an adjustable parameter. Physically we can implement changes in E through the application of appropriate gate potentials. All numerical parameters in the above pieces of H_{so} are those for GaAs found in Ref. 14

The eigenvalue equation $H|\psi\rangle = \epsilon|\psi\rangle$, with H given by Eqs. (12)–(20), was solved numerically to obtain the lowest few eigenvalues and eigenstates vs the various parameters of the system. These parameters include the magnetic-field strength B, the electric field E, and the strength of the quantum dot confinement potential as specified by the quantum dot radius ℓ_o [Eq. (7)].

The notion of electric-field-induced spin switching is quantified by defining an effective electron g factor by the following definition:

$$\epsilon = \frac{1}{2} g \mu_B \sigma_z B \tag{21}$$

to describe the energy difference between the lowest energy up- and down-spin states. Thus we consider the lowest two states (including spin) ϵ_2 and ϵ_1 and calculate the effective g factor as

$$g = \frac{(\epsilon_2 - \epsilon_1)}{\mu_B B}. \tag{22}$$

Results for the variation of this effective g factor as a function of the parameters E, B, and ℓ_o are presented in Sec. III.

III. RESULTS

We now turn to a presentation of the key results of this work: the tunability of the electron g factor through the application of electric and magnetic fields. Figure 7 is consistent with previous published work[14] and illustrates the g-factor tunability vs the strength of the applied electric field and confining potential (as parametrized by the quantum dot radius ℓ_o) for fixed magnetic field ($B = 1T$) for the symmetric quantum dot in the quadratic potential of Eq. (2) with $\alpha = \beta = 1$. We express g relative to its nonrelativistic free-electron value $g_o = 2$. Figure 8 is also consistent with previous published work[14] and illustrates the g-factor tunability vs the strength of the applied electric field and magnetic field for fixed confining potential (parametrized by the quantum dot radius $\ell_o = 20$ nm).

Upon introducing in-plane anisotropy to the confining potential we find significant changes in the electric-field in-

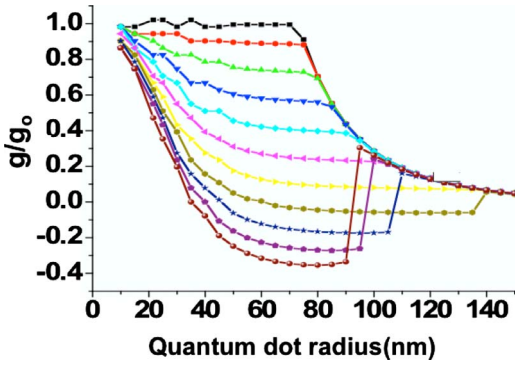

FIG. 7. (Color online) Electric-field-induced changes in the g factor vs quantum dot radius for various electric-field strengths for a symmetric quantum dot in the quadratic potential of Eq. (2). From top to bottom, the curves represent increasing electric-field strength as follows. The first curve corresponds to 1×10^4 V/cm and the rest range from 1×10^5 through 1×10^6 V/cm in equal steps with $B=1T$. This result is consistent with Ref. 14. The parameter g is expressed relative to its nonrelativistic free-electron value $g_o=2$.

duced g-factor tunability for dots larger than roughly 65 nm as illustrated in Fig. 9. This figure was generated by choosing $\alpha=1$ and four values of β, given by $\beta=20$, 40, 60, and 80 in Eq. (2). By comparison of Fig. 9 to Fig. 7 we see that the major effects of anisotropy are for dots roughly larger than 65 nm.

To quantify the effects of in-plane anisotropy, we have carried out a parameter study of the g-factor tunability vs degree of anisotropy and the results are presented in Fig. 10. This figure was generated by fixing the quantum dot radius at $\ell_o=120$ nm and holding $\alpha=1$ while varying β with $B=1T$.

Lastly we consider the results for g-factor tunability for quantum dots in the realistic potential of Figs. 2 and 3 and Eq. (1). Figure 11 illustrates the results for a quantum dot in the realistic potential in comparison to several model potentials. The lowest curve, indicated by filled black squares,

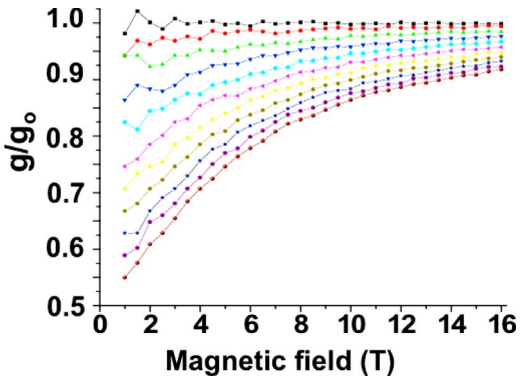

FIG. 8. (Color online) Electric-field-induced changes in the g factor vs magnetic field for various electric-field strengths for the symmetric quantum dot. From top to bottom, the curves represent increasing electric-field strength as follows. The first curve corresponds to 1×10^4 V/cm and the rest range from 1×10^5 through 1×10^6 V/cm in equal steps. For this calculation, the quantum dot radius was fixed at $\ell_o=20$ nm. We express g relative to its nonrelativistic free-electron value $g_o=2$.

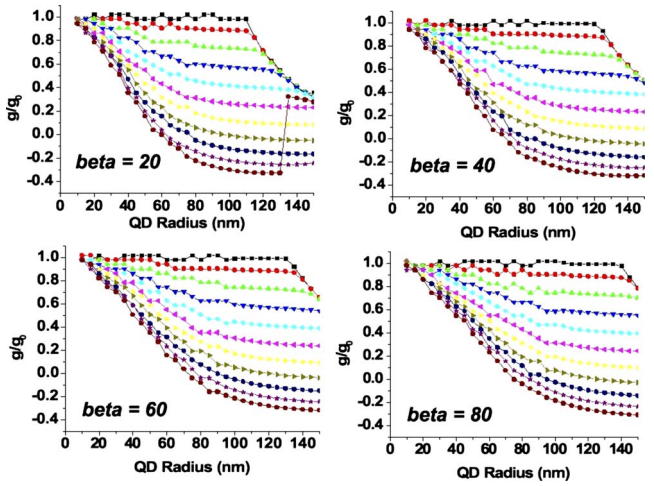

FIG. 9. (Color online) Electric-field induced changes in the g factor vs quantum dot radius for various electric-field strengths for an asymmetric quantum dot for the asymmetric model of Eq. (2) with $\alpha=1$ and $\beta=20$, 40, 60, and 80. In each panel, from top to bottom, the curves represent increasing electric-field strength as follows. The first curve corresponds to 1×10^4 V/cm, and the rest range from 1×10^5 through 1×10^6 V/cm in equal steps. Again we choose $B=1T$. We express g relative to its nonrelativistic free-electron value $g_o=2$.

represents the symmetric model of Eq. (2) with $\alpha=\beta=1$ and the other curves with filled symbols represent varying degrees of anisotropy as follows. The filled red (online) circles represent $\beta=2.8$, while the filled green (online) upward pointing triangles correspond to $\beta=5$ and the blue (online) downward pointing triangles correspond to $\beta=10$. In each case of the quadratic model we have chosen $\ell_o=30$ nm. The results for the realistic potential of Eq. (1) and Figs. 2 and 3 are represented by the open symbols. We see that results for the realistic potential are well represented by the asymmetric

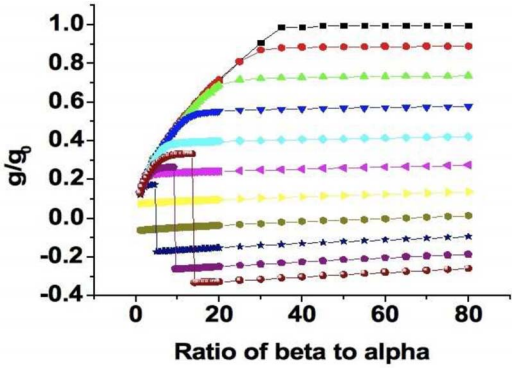

FIG. 10. (Color online) Electric-field-induced changes in the g factor vs the degree of anisotropy of the quantum dot confinement potential for various electric-field strengths. From top to bottom, the curves represent increasing electric-field strength as follows. The first curve corresponds to 1×10^4 V/cm, and the rest range from 1×10^5 through 1×10^6 V/cm in equal steps. This figure assumes the quadratic model of Eq. (2) with $\alpha=1$, $\ell_o=120$ nm, and $B=1T$. We express g relative to its nonrelativistic free-electron value $g_o=2$.

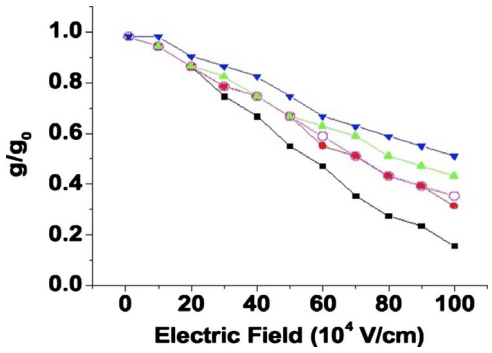

FIG. 11. (Color online) Changes in the g factor vs electric field for quantum dots in the realistic potential of Figs. 2 and 3 [using the form of Eq. (1)] in comparison to results for symmetric and asymmetric model potentials. The black (lowest) curve corresponds to the symmetric model of Eq. (2) with $\alpha=\beta=1$ while the rest of the curves with filed symbols correspond to $\beta=2.8$ (red circles), $\beta=5$ (green upward pointing triangles), and $\beta=10$ (blue downward pointing triangles). In each of these curves corresponding to Eq. (2) we have chosen $\ell_o=30$ nm. The results for the realistic potential are given by the open circles. We note excellent agreement between the $\beta=2.8$ result and that for the realistic potential. We express g relative to its nonrelativistic free-electron value $g_o=2$.

model of Eq. (2) with $\alpha=1$, $\beta=2.8$, and $\ell_o=30$ nm.

The good agreement between the asymmetric model potential and the realistic potential in Fig. 11 is reflected visually in Figs. 6(b) and 6(c) although there are is a slight underestimate of the magnitude of the wave function in Fig. 6(b) in comparison to Fig. 6(c). Obviously, however, from Fig. 11 this slight difference has little effect on the g-factor tunability as evidenced by the close agreement between the filled and open circles in Fig. 11. The quantum dots of Figs. 6(a) and 6(b) correspond to the filled squares and circles of Fig. 11, respectively, emphasizing the importance of anisotropy.

IV. CONCLUSION

We have carried out a numerical simulation study of gate-induced tunability of the electron g factor in a prototype single-electron spintronic device. We consider a realistic three-dimensional geometry and employ a numerical approach based on the finite element method.[47]

The key result of this work is illustrated in Figs. 7 and 9–11: anisotropy in the confining potential significantly extends the size range of quantum dots that exhibit electric-field-induced g-factor tunability. Indeed, in Fig. 7 we see that all of the curves collapse onto a single curve for large quantum dots (i.e., starting around $\ell_o=65$ nm) negating the switching effect. With anisotropy, however, the range of switchability is shifted to larger dots.

Another result of this work is the realization that the degree of anisotropy needs not be very large in order to obtain significant changes in the gate-induced g-factor tunability, as illustrated in Fig. 10. We see that the maximum effect is obtained for dot in the range of $\beta/\alpha \approx 15-25$ nm and begins to decrease slightly for larger values of this shape-anisotropy ratio. The jumps in the value of the g factor from positive to negative value are indicative of level crossings (e.g., the relative ordering of spin-up and -down levels changes as a function of the anisotropy).

Lastly we have seen from Fig. 11 that results for quantum dots in realistic potentials can be well represented by the anisotropic model of Eq. (2) with $\alpha=1$, $\beta=2.8$, and $\ell_o=30$ nm. By employing nonperturbative fully numerical methods and realistic geometries, our approach is providing insights that might be difficult or impossible to obtain using analytical techniques alone.

ACKNOWLEDGMENT

This work was supported by the NRI INDEX center.

[1] D. Loss and D. P. DiVincenzo, Phys. Rev. A **57**, 120 (1998).
[2] H.-A. Engel, L. P. Kouwenhoven, D. Loss, and C. M. Marcus, Quantum Inf. Process. **3**, 115 (2004).
[3] W. A. Coish and D. Loss, Phys. Rev. B **75**, 161302(R) (2007).
[4] *Semiconductor Spintronics and Quantum Computation*, edited by D. D. Awschalom, D. Loss, and N. Samarth (Springer, New York, 2002).
[5] R. Hanson, L. P. Kouwenhoven, J. R. Petta, and S. Tarucha, Rev. Mod. Phys. **79**, 1217 (2007).
[6] I. Zutic, J. Fabian, and S. Das Sarma, Rev. Mod. Phys. **76**, 323 (2004).
[7] S. Bandyopadhyay, Phys. Rev. B **61**, 13813 (2000).
[8] A. R. Trivedi and S. Bandyopadhyay, J. Appl. Phys. **103**, 104311 (2008).
[9] T. Calarco, A. Datta, P. Fedichev, E. Pazy, and P. Zoller, Phys. Rev. A **68**, 012310 (2003).
[10] R. Hanson and D. D. Awschalom, Nature (London) **453**, 1043 (2008).
[11] E. Biolatti, I. D'Amico, P. Zanardi, and F. Rossi, Phys. Rev. B **65**, 075306 (2002).
[12] D. K. Young, J. A. Gupta, E. Johnston-Halperin, R. Epstein, Y. Kato, and D. D. Awschalom, Semicond. Sci. Technol. **17**, 275 (2002).
[13] M. Thorwart and P. Hanggi, Phys. Rev. A **65**, 012309 (2001).
[14] R. de Sousa and S. Das Sarma, Phys. Rev. B **68**, 155330 (2003).
[15] E. I. Rashba and A. L. Efros, Appl. Phys. Lett. **83**, 5295 (2003).
[16] E. I. Rashba and A. L. Efros, Phys. Rev. Lett. **91**, 126405 (2003).
[17] E. A. Laird, C. Barthel, E. I. Rashba, C. M. Marcus, M. P. Hanson, and A. C. Gossard, Phys. Rev. Lett. **99**, 246601 (2007).
[18] C. S. Tang, A. G. Malshukov, and K. A. Chao, Phys. Rev. B **71**, 195314 (2005).
[19] J. Pingenot, C. E. Pryor, and M. E. Flatte, Appl. Phys. Lett. **92**, 222502 (2008).
[20] H. W. Jiang and E. Yablonovitch, Phys. Rev. B **64**, 041307(R) (2001).

[21] Y.-P. Shim and P. Hawrylak, Phys. Rev. B **78**, 165317 (2008).
[22] K. C. Nowack, F. H. L. Koppens, Y. V. Nazarov, and L. M. K. Vandersypen, Science **318**, 1430 (2007).
[23] A. L. Efros, M. Rosen, and E. I. Rashba, Phys. Rev. Lett. **87**, 206601 (2001).
[24] S. Tarucha and J. Baugh, J. Phys. Soc. Jpn. **77**, 031011 (2008).
[25] S. Amasha, K. MacLean, I. P. Radu, D. M. Zumbuhl, M. A. Kastner, M. P. Hanson, and A. C. Gossard, Phys. Rev. Lett. **100**, 046803 (2008).
[26] J.-M. Tang, J. Levy, and M. E. Flatte, Phys. Rev. Lett. **97**, 106803 (2006).
[27] G. Ortner, M. Bayer, Y. Lyanda-Geller, T. L. Reinecke, A. Kress, J. P. Reithmaier, and A. Forchel, Phys. Rev. Lett. **94**, 157401 (2005).
[28] G. Bester and A. Zunger, Phys. Rev. B **72**, 165334 (2005).
[29] A. Högele, S. Seidl, M. Kroner, K. Karrai, R. J. Warburton, M. Atatüre, J. Dreiser, A. Imamoğlu, B. D. Gerardot, and P. M. Petroff, J. Supercond. **18**, 245 (2005).
[30] L. S. Levitov and E. I. Rashba, Phys. Rev. B **67**, 115324 (2003).
[31] M. Governale, F. Taddei, and R. Fazio, Phys. Rev. B **68**, 155324 (2003).
[32] T. Nakaoka, S. Tarucha, and Y. Arakawa, Phys. Rev. B **76**, 041301(R) (2007).
[33] Y. K. Kato and D. D. Awschalom, J. Phys. Soc. Jpn. **77**, 031006 (2008).
[34] M. F. Doty, M. Scheibner, I. V. Ponomarev, E. A. Stinaff, A. S. Bracker, V. L. Korenev, T. L. Reinecke, and D. Gammon, Phys. Rev. Lett. **97**, 197202 (2006).
[35] S. Bednarek, K. Lis, and B. Szafran, Phys. Rev. B **77**, 115320 (2008).
[36] A. Kwasniowski and J. Adamowski, J. Phys.: Condens. Matter **20**, 215208 (2008).
[37] J. Konemann, R. J. Haug, D. K. Maude, V. I. Falko, and B. L. Altshuler, Phys. Rev. Lett. **94**, 226404 (2005).
[38] C. F. Destefani and S. E. Ulloa, Phys. Rev. B **71**, 161303(R) (2005).
[39] G. Dresselhaus, Phys. Rev. **100**, 580 (1955).
[40] Y. A. Bychkov and E. I. Rashba, J. Phys. C **17**, 6039 (1984).
[41] Y. Kato, R. C. Myers, A. C. Gossard, J. Levy, and D. D. Awschalom, Science **299**, 1201 (2003).
[42] T. Andlauer and P. Vogl, Phys. Rev. B **79**, 045307 (2009).
[43] J.-H. Cremers, P. W. Brouwer, and V. I. Fal'ko, Phys. Rev. B **68**, 125329 (2003).
[44] R. Ravishankar, P. Matagne, J. P. Leburton, R. M. Martin, and S. Tarucha, Phys. Rev. B **69**, 035326 (2004).
[45] B. Szafran, F. M. Peeters, and S. Bednarek, Phys. Rev. B **70**, 205318 (2004).
[46] I. L. Aleiner and V. I. Fal'ko, Phys. Rev. Lett. **87**, 256801 (2001).
[47] COMSOL MULTIPHYSICS version 3.4 (www.comsol.com).
[48] F. Stern and S. Das Sarma, Phys. Rev. B **30**, 840 (1984).
[49] B. Schuh, J. Phys. A **18**, 803 (1985).
[50] L. Hedin and B. I. Lundqvist, J. Phys. C **4**, 2064 (1971).
[51] V. Fock, Physik **47**, 446 (1928).
[52] C. G. Darwin, Proc. Cambridge Philos. Soc. **27**, 86 (1931).
[53] E. I. Rashba, Fiz. Tverd. Tela (Leningrad) **2**, 1224 (1960).
[54] M. Dyakonov and V. Kachorovskii, Fiz. Tekh. Poluprovodn. (S.-Peterburg) **20**, 178 (1986).